Development of a Multiscale XGBoost-based Model for Enhanced Detection of Potato Late Blight Using Sentinel-2, UAV, and Ground Data

Sheng Chang, Zelong Chi, Hong Chen, Tongle Hu, Caixia Gao, Jihua Meng and Liangxiu Han

***Abstract*—Potatoes, a crucial staple crop, face significant threats from late blight, which poses serious risks to food security. Despite extensive research using ground and unmanned aerial vehicle (UAV) hyperspectral data for crop disease monitoring, satellite-scale identification of diseases like Potato Late Blight (PLB) remains limited. This study employs a multi-scale analysis approach, integrating high-resolution Sentinel-2 multispectral satellite data with UAV and ground spectral data, to monitor and identify PLB. A key finding of this study is the general similarity in spectral patterns across different scales, with consistent valley values in bands of Blue and Red and peak values in bands of Near Infrared and Narrow near Infrared, accompanied by a consistent decrease in reflectance correlating with increasing disease severity. Furthermore, the study highlights scale-dependent spectral variations, with changes in bands of Vegetation Red Edge2, Vegetation Red Edge3, Near Infrared and Narrow Near Infrared being more pronounced at the ground scale compared to UAV and satellite scales. Based on the developed Red Edge Index and Disease Stress Index with a suite of machine learning algorithms, we proposed a XGBoost-based model integrating spectral indices for PLB monitoring (PLB-SI-XGBoost). Notably, the proposed model demonstrated the highest average evaluation score of 0.88 and the lowest root mean square error (RMSE) of 13.50 during ground scale validation, outperforming other algorithms. At the UAV scale, the proposed model achieved a robust R-squared value of 0.74 and an RMSE of 18.27. Moreover, the application of Sentinel-2 data for disease detection at satellite scale yielded an accuracy of 70% in the model. The results of the study emphasize the importance of scale in disease monitoring models and illuminate the potential for satellite-scale surveillance of PLB. The exceptional performance of PLB-SI-XGBoost model in detecting PLB suggests its utility in enhancing agricultural decision-making with more accurate and reliable data support.**

***Index Terms*— Hyperspectral remote sensing, Multispectral remote sensing, Potato late blight, XGBoost, Machine learning, Sentinel-2, Multiscale.**

This work was supported in part by the National Key R&D Program of China under grant 2017YFE0122700, and in part by the National Natural Science Foundation of China under Grant 42271406. *(Corresponding author: Hong Chen, Tongle Hu)*.

Sheng Chang is with the Key Laboratory of Remote Sensing and Digital Earth, Aerospace Information Research Institute, Chinese Academy of Sciences (AIRCAS), Beijing 100101, China (e-mail: changsheng@aircas.ac.cn).

Zelong Chi is with the Key Laboratory of Biodiversity and Environment on the Qinghai-Tibetan Plateau, Ministry of Education, Tibet University, Lhasa,850000, China (e-mail:chizelong66@163.com).

Hong Chen is with the China Aero Geophysical Survey and Remote Sensing Center for Nature Resources, Beijing, 100083, China (e-mail: chch1223@126.com).

Tongle Hu is with the College of Plant Protection, Hebei Agriculture University, Baoding, 070001, China (e-mail: tonglemail@163.com).

Caixia Gao is with the National Engineering Laboratory for Satellite Remote Sensing Applications, Aerospace Information Research Institute, Chinese Academy of Sciences (AIRCAS), Beijing 100101, China (e-mail: gaocx@aircas.ac.cn).

Jihua Meng is with the Key Laboratory of Digital Earth Science, Aerospace Information Research Institute, Chinese Academy of Sciences, Beijing 100101, China (e-mail: mengjh@aircas.ac.cn).

Liangxiu Han is with the Department of Computing and Mathematics, Faculty of Science and Engineering, Manchester Metropolitan University, Manchester M1 5GD, UK (e-mail: L.Han@mmu.ac.uk).

I. Introduction

In 2016, China introduced the "Potato Staple Food Strategy", aiming to industrialize and elevate the status of potatoes within the national diet. This initiative anticipates that half of the projected increase in China's grain production over the next two decades will be attributed to potatoes [1]. Potatoes play a crucial role in agricultural innovation and the shift towards sustainable Agriculture 4.0 practices. However, historical devastation such as the "Irish Potato Famine" in the 1840s and a severe potato blight in China's Sichuan and Chongqing regions in the 1940s, which led to an 80% reduction in yields, underscore the significant threat posed by potato late blight (PLB). Recognized as one of the most severe plant diseases globally, the threat of PLB remains substantial [2]. Traditional methods for monitoring PLB rely on field inspections conducted by agricultural practitioners or technicians. These methods are labor-intensive and susceptible to misdiagnosis. The advent of remote sensing technology in the early 1930s [3] introduced new possibilities for disease monitoring by exploiting the distinct spectral reflection characteristics of healthy and diseased plants across various bands [4, 5].

Remote sensing efficacy in crop disease monitoring depends on detecting stress-induced symptoms via specialized sensors [6], enabling the development of models to assess disease severity. These models start with the analysis of spectral bands and their response functions. The spectral response to diseases is complex and can be described as a function of various crop changes [7], such as alterations in pigmentation, water content, morphology, and structure. These multivariate effects are disease-specific [8-10]. Vegetation indices, derived from algebraic operations on spectral data within sensitive bands, can reveal the pathophysiological spectral characteristics of crops, facilitating disease monitoring [11, 12]. As a result, different diseases, each with their unique spectral signatures, require tailored remote sensing strategies for effective monitoring.

In the case of potato canopies, the reflectance within the 680-750nm wavelength range gradually increases, with near infrared (NIR) reflectance notably higher than in the visible spectrum. Late blight infection in potatoes leads to significant changes in reflectance between 750-1350nm, where the severity of the disease correlates with a varying decrease in reflectance [13]. The variability in reflectance in the infrared region is more pronounced than in the visible region, attributed to the disease's impact on the plant's physiological responses, such as changes in chlorophyll content and alterations in the leaf's internal structure [14]. A decrease in chlorophyll content results in lower absorption in the red light spectrum, subsequently increasing the reflectance of infected plants. Conversely, the reflectance in the NIR region decreases due to changes in the leaf's internal structure.

Extensive research has been dedicated to detecting PLB, including the use of hyperspectral imaging under laboratory conditions [15], and building of the correlations between indoor and field models through hyperspectral databases [16]. Field spectroscopic studies were performed using a handheld field spectrometer to examine spectral variability between healthy and late blight-infected potato canopies [17]. These studies focus on assessing which spectral variables and at which time of late blight can be detected over potato crops by field spectroradiometer has been the focus of several studies [18]. However, they are typically limited to assessments at leaf canopy-level, posing challenges for comprehensive monitoring across large region.

To address these challenges, researchers have increasingly utilized Unmanned Aerial Vehicles (UAVs) equipped with diverse camera technologies for rapid, high-resolution image acquisition. This approach includes techniques for assessing PLB severity through UAV-captured RGB images [19], and the deployment of several indices [9] or deep learning models to automate PLB diagnosis from UAV hyperspectral imagery [13, 20]. Despite these technological advances, UAV-based methods face constraints in flight endurance and coverage areas, while the limited availability of reliable satellite data hampers the scope of satellite-scale monitoring capabilities. In recent years, satellite remote sensing has gained prominence as a feasible alternative for crop disease monitoring. Notable applications include the detection and monitoring of wheat diseases using Quickbird and SPOT-6 imagery [21], alongside the effective employment of Sentinel-2 data for monitoring wheat powdery mildew in China, where monitoring accuracies have reached up to 78% [22].

Despite the advancements in remote sensing technology, satellite-scale identification of PLB remains underexplored, with much of the current research focus on UAV-scale data. This limitation restricts the potential for extensive, convenient monitoring of the disease. Machine learning techniques have increasingly been leveraged to tackle the challenge of PLB in recent years. In a pivotal study by Duarte-Carvajalino et al. [23], a thorough assessment of late blight across 14 potato genotypes was performed using UAV-derived multispectral imagery in conjunction with machine learning approaches. These included multilayer perceptrons, convolutional neural networks, SVM, and RF. The findings indicated that machine learning algorithms are a viable alternative to traditional visual estimation methods, achieving an average absolute error of 11.72%, which is deemed acceptable for real applications. In another study, Sun et al. [24] compared and developed models for monitoring the severity of PLB using SVM, RF, and KNN algorithms. The success of these classifications have shed light on the potential of machine learning in addressing PLB issues.

The current study introduces a method for detecting PLB through the analysis of multiscale imagery. Several disease indices are developed and seven coupled machine learning models are trained using high-quality ground-based PLB spectral data and disease metrics. These models are then employed for classification and regression on new datasets, followed by monitoring and validation at ground, UAV and satellite scales. To evaluate the effectiveness of integrating machine learning algorithms with remote sensing data, a comparative analysis was conducted using ground-based datasets. The aim of this comparative analysis is to explore the feasibility of satellite-scale monitoring of PLB using spectral information. The proposed model is expected to contribute to the development of more rational and effective decision-making systems for PLB management. The study will address the following questions:

(1) Are the spectral patterns associated with PLB consistent across various spatial scales?

(2) How do the performances of ground data-based PLB monitoring models vary across different scales?

(3) What is the feasibility of extending PLB detection by integrating machine learning model with remote sensing to satellite scale?

Ⅱ. Description of the Study Area and Data Sets

A. Study Area

Considering the availability of historical data and the ease of acquiring meteorological and ground-level data, the study area includes the Guyuan county in Northern Hebei province and the Duolun county in Middle-South of Inner Mongolia

Autonomous Region. These regions are recognized as principal potato production areas in northern China (Fig. **1**). The potato cultivation cycle in these regions typically begins with the sowing and emergence stages from April to May, progresses through a rapid growth phase from June to August, and culminates in the harvesting season from late August to September. Two counties are situated in a temperate continental climate zone, characterized by rising summer temperatures, ample rainfall, and high humidity—conditions that are favorable for the development of PLB [25]. The climatic factors, coupled with the region's critical role in potato production, make it as an ideal study area for research on modeling and experimental validation of the PLB monitoring.

B. Ground Data Collection and Preprocessing

To evaluate the impact of multi-scale disease, this study utilized two different types of ground experimental data: controlled small-area experiments and field observations, to construct and validate the proposed model. Fig. 1 details the spatial distribution of observation data sampling points within the study area.

1) Controlled small-area experiments: This study conducted experiments (S1 and S2) at locations in Sirenwa Township (41.684003N, 115.746497E) and Shandianhe Township (41.700667 N, 115.795664E) within Guyuan County, as shown in Fig. 1, with the red triangles indicating the locations where ground data were collected. The first small-area experiment consisted of 9 plots, while the second involved 16 plots, each plot measuring 1m × 1m. In the first small-area experiment, two potato varieties 'Yizhangshu No.12' and 'Shishu No.1' were planted. Two control groups and four infection groups were established, with seedlings infected starting on May 13, 2020, at a spore concentration of 9mg/100mL.

The second small-area experiment consisted of 6 control groups and 30 infection groups, with the infection process beginning on May 14, 2020, using the same spore concentration as in the first experiment. Field spectral data for two areas were collected by the SVC HR-1024i full-band spectral radiometer under cloudless conditions between 10:00 and 14:00 on August 16, 2020. The initial hyperspectral measurements obtained from the radiometer were corrected and registered based on predefined marked positions. The raw data were preprocessed using SVC HR-1024i PC-side software, facilitating the export of full-band dataset. Simultaneously, PLB severity were observed in each 0.2m × 0.2m sample area using the methods [2, 26] shown in Table **I**. In total, 623 pairs of high-quality ground spectral and disease data were collected, which are essential for capturing micro-environmental conditions at the plot level and constructing the PLB monitoring model.

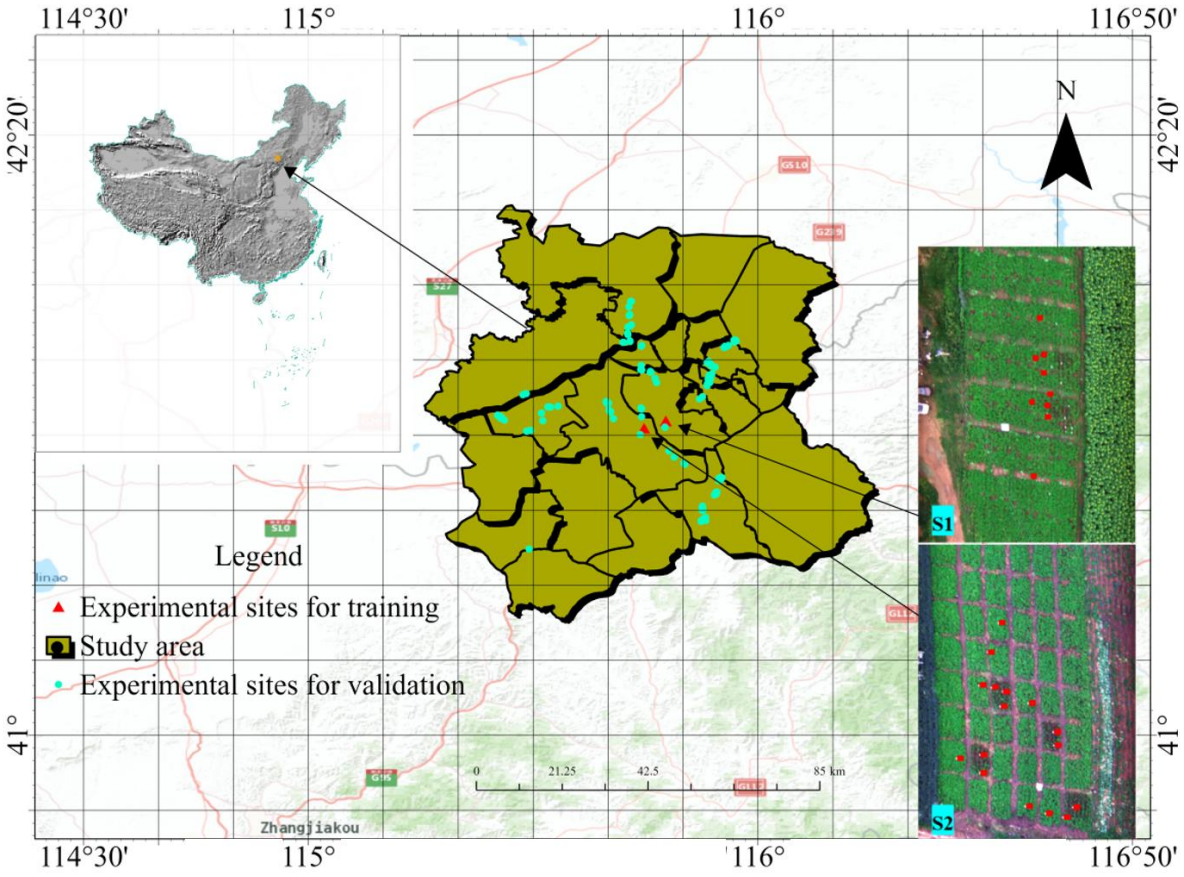

Fig. 1. Presents a detailed geographic profile of the study area, illustrating the spatial distribution of the sampling points and plots.

TABLE I
A METHOD FOR VISUAL ESTIMATION OF PLB DISEASE IN THE FIELD

SEVERITY	DESCRIPTION
0.0%	No disease is observed.
0.1%	First sporulating lesion in the plot
1.0%	General light infection observed, approximately 5-10 lesions per plant
5.0%	Approximately 50 lesions per plant, affecting 1 in 10 leaflets.
5.0%	Nearly every leaflet is infected, but plants retain normal form; a blight odor may be present. Field appears green, though every plant is affected.
50.0%	Every plant is affected, with approximately 50% of the leaf area destroyed. Field appears green flecked with brown.
75.0%	Approximately 75% of the leaf area is destroyed; field appears neither predominantly green nor Brown.
95.0%	Only a few leaves remain on plants, but stems are still green.
100.0%	All leaves are dead, and the stems are either dead or dying.

To ensure the compatibility of ground-based hyperspectral data with Sentinel-2 satellite data, a weighted averaging method was applied to align it with specific Sentinel-2 bands, namely B2, B3, B4, B5, B6, B7, B8, B8A, B11, and B12 (as shown in Table II). This processing step is crucial for the direct comparison, validation, and analysis between ground spectral data and satellite observation data. Additionally, the Z-score method was employed for outlier detection to eliminate the influence of extreme values on the data distribution, ensuring the robustness and accuracy of data processing.

$$Rx_{S2} = \frac{R1_{SVC} * w1 + R2_{SVC} * w2 + R3_{SVC} * w3 + \cdots + Rn_{SVC} * wn}{w1 + w2 + w3 + \cdots + wn} \quad (1)$$

Here, Rx_{S2} represents the composite value of spectral reflectance from SVC HR-1024i ground observations corresponding to the band ranges of Sentinel-2 satellite data. $R1_{SVC}$, $R2_{SVC}$, $R3_{SVC}$, ... and Rn_{SVC} represent the spectral reflectance of multiple narrow bands included within the band range of SVC, and $w1$, $w2$, $w3$, ...and $w4$ present the width of each narrow band.

2) Field observation data: The cyan dots on the map in Fig. 1 represent the sampling locations at the regional scale, distributed across multiple sites labeled the study area. Field observations were conducted from August 12 to 13, 2021, collecting a total of 201 field observation data. GPS was used to mark the different sampling locations, with each observation area corresponding to the spatial resolution of Sentinel-2 pixels (10m×10m). The severity of disease within each pixel was determined using visual estimation methods, with the assessment criteria detailed in Table **I**.

C. Remote Sensing Data and Processing

The Sentinel-2 satellite constellation, developed and launched by the European Space Agency (ESA), provides high-resolution multispectral imaging. It comprises two satellites, Sentinel-2A and Sentinel-2B, each with a revisit 10-day revisit period，which combine to offer a 5-day revisit period. Equipped with a Multispectral Instrument (MSI), Sentinel-2 provides imagery across 13 spectral bands,including four with a 10-meter resolution (blue, green, red, and near-infrared), six with a 20-meter resolution (three red-edge bands and one near-infrared band), and three with a 60-meter resolution(as depicted in Table Ⅱ). In this study, a total of 10 bands spanning from the visible light to the shortwave infrared spectrum were utilized, encompassing both 10-meter and 20-meter resolutions. Sentinel-2's data products are derived from Google Earth Engine (GEE) [20], utilizing self-contained QA60 band de-cloudings to improve image quality [27].

This study also utilized a full-band imaging spectroradiometer, the HR-1024i, mounted on a DJI Matrice 600 Pro, to collect UAV-derived spectral data within the range of 350nm to 2500nm at the flight altitude of 100m. The UAV observations were conducted simultaneously with ground measurements, collecting spectral reflectance data of potato canopies in sampling areas S1 and S2 with 0.2m resolution, along with corresponding photographs. The collected data were processed to align with the wavelength range of Sentinel-2 (400-1000nm), generating 25 data pairs that included spectral values and disease severity information.

III. METHODOLOGY

The main processes of the proposed model for wide-area monitoring of PLB include data collection, disease index calculation, model construction, model validation, and optimization, as shown in Fig. **2**.

A. Disease Indices Based on Remote Sensing Spectra

In this study, high-spectral-resolution ground-based reflectance data were first synthesized into broadband reflectance to match the spectral response of Sentinel-2 satellite data across different wavelength ranges. This synthesis facilitated in analyzing the correlation between synthesized broadband reflectance with the incidence of PLB，evaluating the sensitivity of different broadband reflectance to the disease. Based on the spectral reflectance differences under various PLB infection rates, four most sensitive bands (R_{RedE2}, R_{RedE3}, R_{NIR}, R_{RedE4}) were used to construct indices, which were further analyzed for sensitivity.

Previous research [28, 29] has demonstrated that UAV hyperspectral data within specific bands (including 540nm, 610nm, 620nm, 700nm, 710nm, 730nm, 780nm, and 1040nm) can effectively distinguish between healthy potatoes and those affected by PLB. Notably, when the infection rate reaches 25%, bands at 710nm, 720nm, and 750nm become particularly effective for differentiation. This suggests that the red-edge bands are highly indicative of the PLB severity. The shape and position of the red edge are significant as they

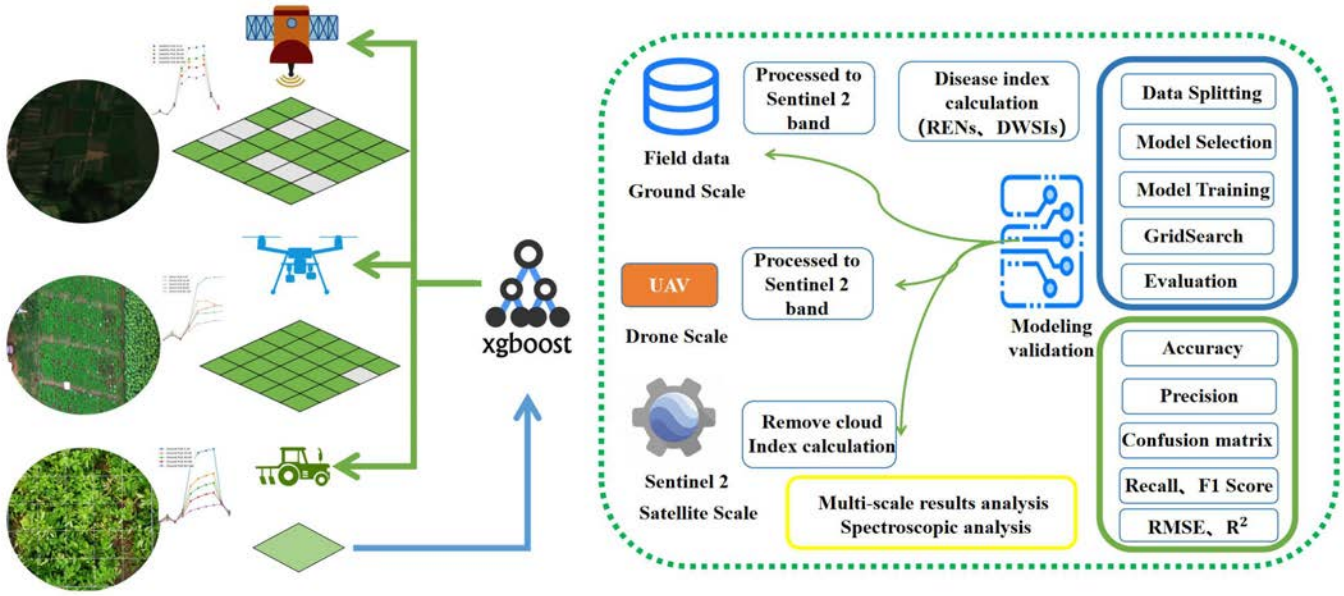

Fig. 2. Workflow for integrated PLB monitoring method

TABLE II
THE SPECIFIC PARAMETER INFORMATION OF THE SENTINEL- 2 BANDS

Band No.	Band name	Sentinel-2A Central wavelength (nm)	Sentinel-2B Central wavelength (nm)	Band width (nm)	Resolution (meters)
1	B1	443.9	442.3	20	60
2	B2	496.6	492.1	65	10
3	B3 (Green)	560	559	35	10
4	B4 (Red)	664.5	665	30	10
5	B5 (R_{RedE1})	703.9	703.8	15	20
6	B6 (R_{RedE2})	740.2	739.1	15	20
7	B7 (R_{RedE3})	782.5	779.7	20	20
8	B8 (R_{NIR})	835.1	833	115	10
8b	B8A (R_{RedE4})	864.8	864	20	20
9	Water Vapour	945	943.2	20	60
10	SWIR-Cirrus	1373.5	1376.9	30	60
11	B11 (R_{swir1})	1613.7	1610.4	90	20
12	B12 (R_{swir2})	2202.4	2185.7	180	20

reflect changes in chlorophyll content and leaf structure. This is due to chlorophyll's strong absorption in the red band and strong scattering in the near-infrared region within leaf tissues [30, 31]. To detect PLB areas, multiple red-edge bands were used to formulate red-edge indices. The specific red-edge indices established are as follows:

$$RENI1 = \frac{R_{RedE2} - R_{RedE1}}{R_{RedE2} + R_{RedE1}} \quad (2)$$

$$RENI2 = \frac{R_{RedE3} - R_{RedE1}}{R_{RedE3} + R_{RedE1}} \quad (3)$$

$$RENI3 = \frac{R_{RedE4} - R_{RedE1}}{R_{RedE4} + R_{RedE1}} \quad (4)$$

Where R_{Red} represents the reflectance in the red band, R_{RedE1}、R_{RedE2}、R_{RedE3}、R_{RedE4} represent the reflectance in the four red-edge bands, and R_{NIR} represents the reflectance in the near-infrared band.

Additionally, the Disease Water Stress Index (DWSI) was introduced, which is a spectral reflectance sensitive to changes in leaf pigments, internal leaf structure, and moisture content [32]. DWSI consists of the green band, red band, near-infrared, and shortwave infrared. Corresponding to various bands of Sentinel-2, multiple indices were proposed using a similar method, replacing R_{NIR} with R_{RedE2}, R_{RedE3}, and R_{RedE4}, resulting in the following indices:

$$DWSI2 = \frac{R_{RedE2} - R_{Green}}{R_{SWIR1} + R_{Red}} \quad (5)$$

$$DWSI3 = \frac{R_{RedE3} - R_{Green}}{R_{SWIR1} + R_{Red}} \quad (6)$$

$$DWSI4 = \frac{R_{RedE4} - R_{Green}}{R_{SWIR1} + R_{Red}} \quad (7)$$

Where R_{Green} represents the reflectance in the green band (B3), and R_{SWIR1} represents the reflectance in the short wave infrared band (B11).

B. Alternative Machine Learning Methods

To effectively construct the proposed PLB monitoring model, seven machine learning algorithms were employed. Below (Table **III**) is a concise list explaining the machine

learning algorithms evaluated in the study.

TABLE III
ALTERNATIVE ALGORITHMS AND INTRODUCTIONS

ALGORITHM	DESCRIPTION
Random Forest (RF)	An ensemble of decision trees that operate on the majority-vote principle for classification or average predictions for regression [33].
Gradient Boosting (GB)	Sequentially trains weak learners, focusing on the residuals of the previous model, refining predictions through gradient descent [34].
K-Nearest Neighbors (KNN)	A non-parametric algorithm that uses the 'K' closest neighbors in the training set for classification or prediction [35].
Neural Network (NN)	Inspired by biological neural networks, capable of capturing complex, nonlinear relationships through interconnected layers of neurons [36].
Support Vector Machine (SVM)	Identifies an optimal hyperplane for class separation in feature space, using kernel functions for nonlinear data [37].
eXtreme Gradient Boosting (XGBoost)	A variant of gradient boosting that introduces regularization and parallel computing to improve efficiency and performance [38].
Categorical Boosting (CatBoost)	Specifically designed for classification problems, with technology for automatic transformation of categorical features and robust generalization [39].

C. Multi-scale disease severity-spectral pattern and sensitivity analysis methods

In this study, we employed Spearman's rank correlation coefficient [40] to examine the relationship between the severity of Potato Late Blight (PLB) and spectral reflectance patterns. By ranking the data and calculating the coefficient, we were able to determine the degree of association between the spectral characteristics and disease progression without assuming a specific distribution of the data. This methodological choice was critical for our analysis, as it allowed us to include all relevant data points and provided a robust measure of correlation that is not influenced by outliers or data distribution.

To investigate the relationship between disease severity and spectral patterns across various scales, and to compare them for these scales in the context of late blight progression, we synthesized data from three distinct scales. This synthesis included alternative indices — excluding the UAV band's missing data—and it was based on the reflectance values of Sentinel-2 satellite bands. Additionally, we incorporated the aggregate of six disease indices (excluding the UAV band's missing segment). We then analyzed the sensitivity and correlation of each index to changes in disease severity using the correlation coefficient. During the visualization process, variables were ordered according to the eigenvalues of the matrix. These eigenvalues signify the extent of variation within the matrix, and by sorting them, we were able to cluster variables with higher correlations, thereby enhancing the clarity of the correlational structure.

D. Construction of PLB monitoring model

This study is dedicated to establishing a monitoring model for PLB , achieved through a series of meticulously designed steps. Initially, spectral data from potato canopies across the visible and near-infrared spectrum were collected using ground spectroradiometers, UAV spectroradiometer, and satellite sensors. With this high-quality ground observation data, a machine learning model was trained to identify and learn the spectral characteristics of PLB. The model was then executed on new datasets to perform classification and regression tasks, predicting disease occurrence. Results were validated at ground, UAV and satellite scales to ensure its accuracy and applicability.

To evaluate the performance of different algorithms, a comparative analysis was conducted based on ground data, testing seven machine learning models: RF, GB, KNN, NN, SVM, XGBoost, and CatBoost. The inputs to the models were spectral bands and indices from the ground measurement and spectral data, and the outputs were disease severity, quantified on a scale of 0 to 100 for regression analysis, or categorized into five classes based on 20-unit intervals for classification.

E. Model evaluation methods

For evaluating the performance of machine learning models [41] in both classification and regression scenarios, the following evaluation methods were adopted:

1) Evaluation Method for classification model: In predicting PLB at the satellite scale, the classification model to determine whether plants were affected by late blight was developed. To evaluate the performance of the classification model, the following metrics were used:

Accuracy: refers to the ratio of the number of samples correctly predicted by the model to the total number of samples.

$$Accuracy = \frac{TP + TN}{TP + TN + FP + FN} \tag{8}$$

Precision: refers to the proportion of plants that the model predicts to be affected by late blight that are actually affected.

$$Precision = \frac{TP}{TP + FP} \tag{9}$$

Recall: the proportion of plants that the model correctly detects for late blight. It tells us how successfully the model can predict how many plants will actually be infested.

$$Recall = \frac{TP}{TP + FN} \tag{10}$$

F1 Score: The F1 score is a blended average of precision and recall, which combines the accuracy and recall of the model.

$$F1 = \frac{Precision \times Recall}{Precision + Recall} \tag{11}$$

Confusion Matrix: is a 2×2 matrix that visualizes the performance of a classification model. It contains the number

of TP,TN, FP, and FN.

Here, TP (True Positive) is the number of true examples, TN (True Negative) is the number of true negative examples, FP (False Positive) is the number of false positive examples, and FN (False Negative) is the number of false negative examples.

2) Evaluation Method for regression model: In addition to the classification model, we also built a regression model to predict continuous changes such as the degree of PLB. For the evaluation of the regression model, the following indicators were used:

The R-square (coefficient of determination), Root Mean Square Error (RMSE) and Mean Square Error (MSE) were chosen to evaluate the goodness-of-fit of the regression model as follows:

$$R^2 = 1 - \frac{\sum_{i=1}^{n}(y_i - \hat{y}_i)^2}{\sum_{i=1}^{n}(y_i - \bar{y})^2} \tag{12}$$

$$RMSE = \sqrt{\frac{1}{n}\sum_{i=1}^{n}(y_i - \hat{y}_i)^2} \tag{13}$$

$$MSE = \frac{1}{n}\sum_{i=1}^{n}(y_i - \hat{y}_i)^2 \tag{14}$$

Where y_i is the observed value, while $\hat{y}_i$ is the model prediction, and n is the sample size.

Besides, five-fold cross-validation is a commonly used model evaluation method that divides the dataset into five subset, one subset is used as the validation set, and the rest as the training set, and the model training and validation are repeated. The five-fold cross-validation R-squared is the average of the R-squared values obtained from each iteration, providing a robust estimate of the model's performance.

$$CV_5 = \frac{1}{5}\sum_{i=1}^{5} eval_i \tag{15}$$

Where, $eval_i$ is the evaluation index of the ith verification, such as accuracy, precision, recall, etc.

III. Result

A. Spectral characteristics of PLB in ground-UAV-satellite scale

This study utilized data from ground-based experiments, UAV, and satellites to explore the spectral variations indicative of PLB across the potato canopy. The results are illustrated in Fig. 3 and Fig. 4.

1) Consistency Across Scales: The spectral reflectance trends observed across the ground, UAV, and satellite scales exhibit a consistent pattern (Fig. **3**). This pattern includes a valley value in the B2 and B4 bands, a peak in the B8 and B8A bands, and an overall consistency in the shape of the spectral reflectance curves. Additionally, the reflectance values of the original bands show general similarity, with a notable decrease in reflectance for B6, B7, B8, and B8A bands as the disease severity increases. Different levels of disease severity correspond to varying degrees of reflectance reduction. Despite these variations, the result illustrates the relative consistency in the spectral response to PLB across different observation scales.

2) Scale-Dependent Spectral Variations: As the severity of late blight increases, the spectral values at the ground scale, especially in bands of B6, B7, B8, and B8A, exhibit more pronounced changes compared to those observed at the UAV and satellite scales. Although the trend in the spectral curve changes remains consistent across different scales, there is a significant variation in the actual reflectance values observed. Fig. **3** illustrates the UAV-derived spectral curves exhibit a narrower bandwidth and some gaps, likely due to the limitations in the spatial resolution and data capture continuity of UAV sensors compared to satellite systems. On the band values of REN1, REN2, REN3 (Fig. **4**), near the ground (0.25-0.5), UAV (0.2-0.55), satellite (0.4-0.6). The ground and the UAV scale show similarity, and the difference with the satellite scale is manifested in the upper and lower limits of the satellite scale are increased.The spectral values close to the ground, UAV, and satellite ranged from 0.25-0.5, 0.2-0.55, and 0.4-0.6, respectively.The spectral values of the ground and UAV scales are similar, and the upper and lower limits of the satellite scale are wider. UAV-derived data are capable of providing more detailed spectral information.

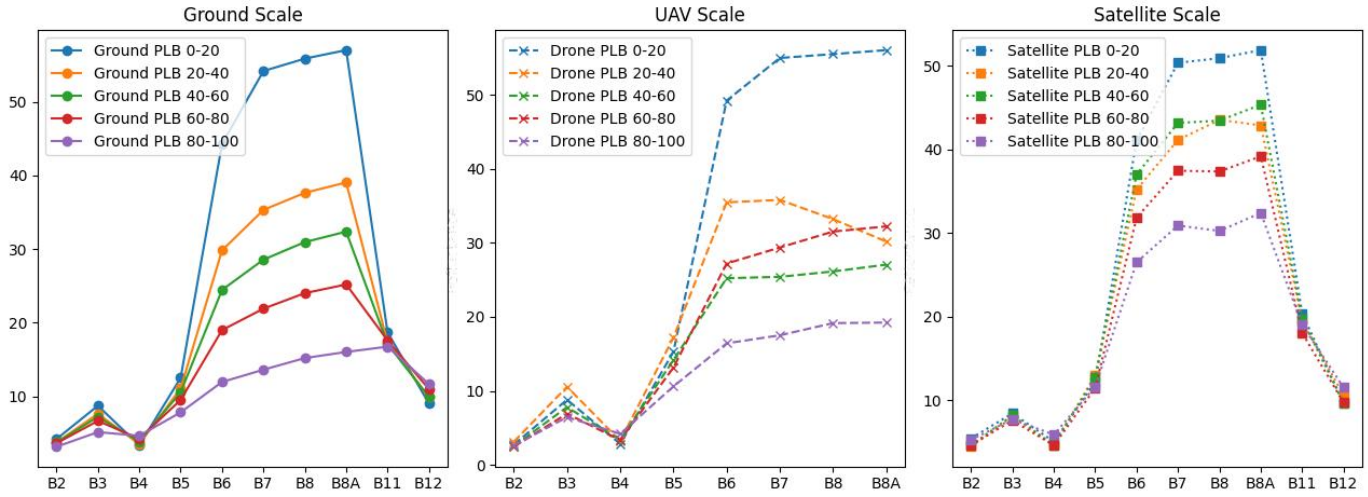

Fig. 3. Spectral response curves of potato canopies affected by PLB in ground, UAV and satellite scale

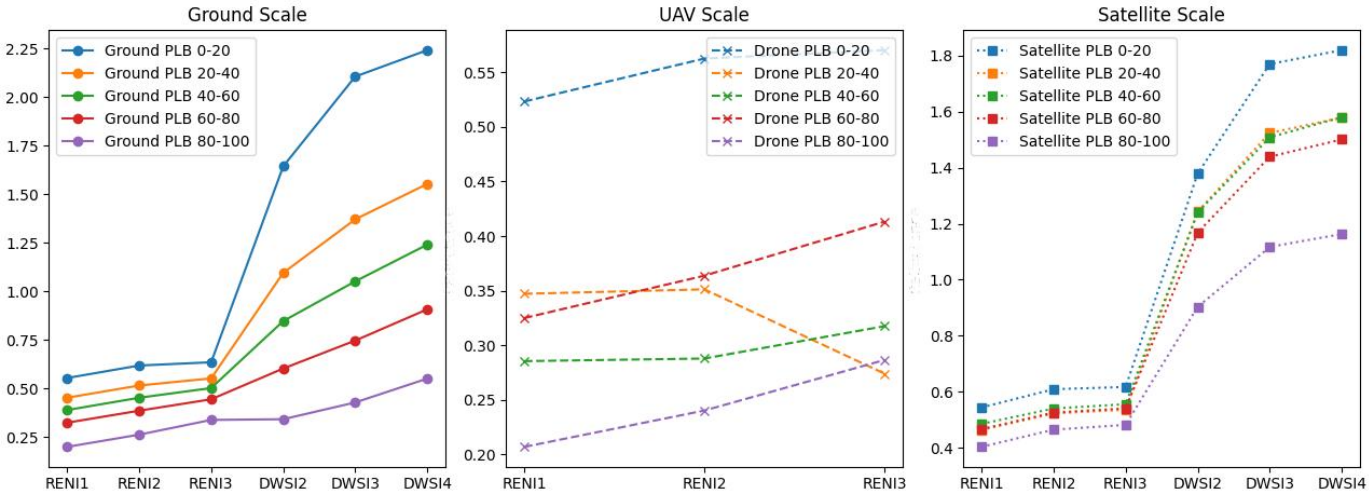

Fig. 4. Spectral indices curves of potato canopies affected by PLB in ground, UAV and satellite scale.

B. Multiscale sensitivity analysis of PLB to spectral characteristics

1) Ground-scale correlation analysis

In the ground-scale correlation matrix depicted in Fig. **5**, a non-statistically significant positive correlation is observed between disease severity and bands B12 and B4. Conversely, a statistically significant negative correlation is evident with remaining bands, particularly with the near-infrared, red-edge bands and derived indices. This relationship is characterized by a negative correlation coefficient exceeding -0.9. These findings suggest that at the ground scale, as the severity of PLB increases, there is a corresponding decrease in the reflectance values of the red edge, near-infrared bands, and derived indices.

2) UAV-scale correlation analysis

In the UAV-scale correlation plot shown in Fig. **6**, a strong negative correlation is observed between disease severity and the three calculated indices, as well as between the red edge and near-infrared bands. These relationships confirm the spectral analysis results, indicating a significant correlation between PLB severity and spectral data. At the UAV scale, PLB was positively correlated with the B4 band, weakly correlated with B2, B3 and B5, and strongly negatively correlated with other bands. Statistical analysis reveals a significant negative correlation, with values ranging from -0.89 to -0.74. The positive correlation for the B4 band suggests that an increase in reflectivity in this band is associated with a increase in disease severity, possibly linked to certain spectral signatures of the plant health.

3) Satellite-scale correlation analysis

The statistically significant relationship between disease severity and the red edge and near-infrared bands is observed to be lower at the satellite scale compared to the ground and UAV scales (Fig. **7**). Specifically, the negative correlation coefficient falls within the range of -0.4 to -0.5, indicating a weaker association. Furthermore, the negative correlations observed among some bands are even less pronounced and do not reach statistical significance. These findings align with the spectral analysis results, which also reveal a more subdued alteration in the spectral reflectance curves compared to the ground and UAV scales. This suggests that,

at the satellite scale, there is a slight decrease in the spectral reflectance values of the red edge and near-infrared bands as the PLB severity increases.

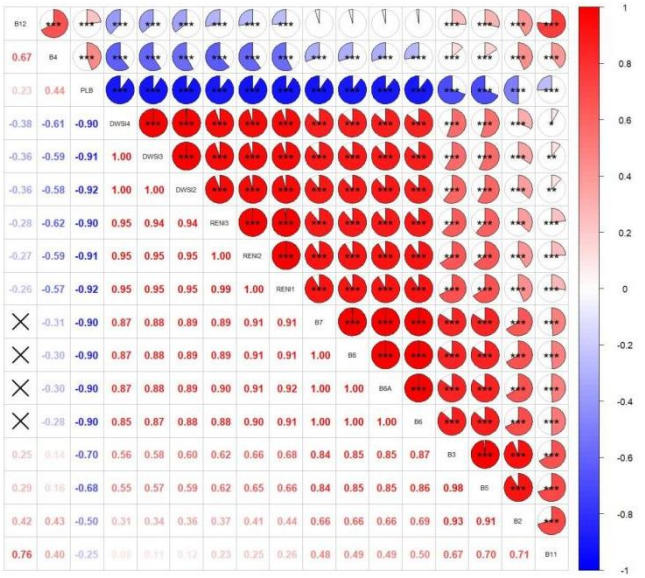

Fig. 5. Ground-scale Correlations between PLB Severity and Spectral Bands/Indices of the Potato Canopy. Figure 5 illustrates the ground-scale correlations between the severity of Potato Late Blight (PLB) and various spectral bands and indices derived from field measurements of the potato canopy. The color bars indicate the strength of the correlation, ranging from blue for negative to red for positive. Significance levels are denoted by asterisks: *p<0.05, **p<0.01, ***p<0.001.

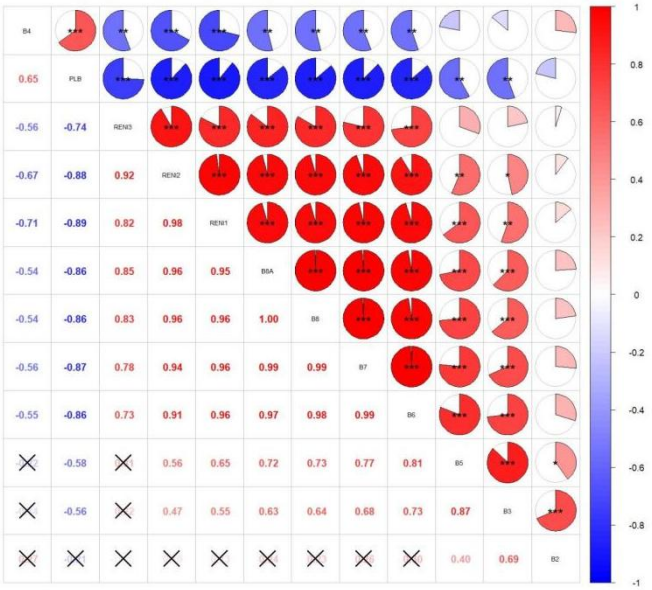

Fig. 6. Correlations between PLB severity and UAV spectral bands/indices. Color bars indicate correlation strength: blue (negative) to red (positive). Asterisk denote significance levels: *p<0.05,**p<0.01,***p< 0.001.

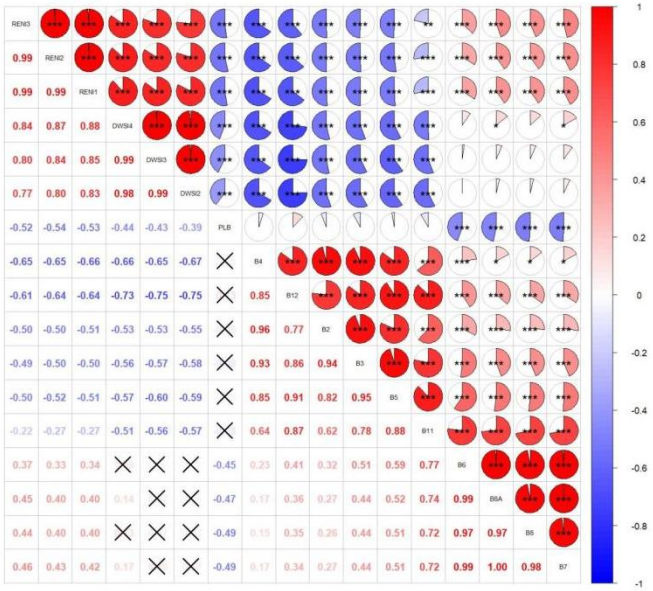

Fig. 7. Correlations between PLB severity and Sentinel-2 spectrual bands/indices. Color bars indicate correlation strength: blue (negative) to red (positive). Asterisk denote significance levels: *p<0.05 ,**p<0.01,***p< 0.001.

4). *Analysis of disease occurrence law of inter-scale spectroscopy*

This study identified a correlation between ground data and the incidence of PLB, as well as between remote sensing data and the incidence of PLB across varying scales, as illustrated in Fig. **8**. Generally this correlation weaken with the expansion of the scale. At the ground scale, a correlation was detected between disease severity and 14 spectral bands or indices (All 14 bands are p< 0.001). In contrast, at the UAV and satellite scales, the number of correlated bands or indices was reduced to 9 (Seven of the bands p< 0.001 and two bands p< 0.01) and 4 (All four of these bands are p< 0.001), respectively. This reduction underscores the variability in correlation intensity across different scales. Additionally, the study observed a negative correlation between the PLB severity and the spectral responses in bands B6, B7, B8, and B8A, with the correlation weakening as the scale increases. These insights highlight the relationship between spectral signatures and the occurrence of PLB, as well as the distinctive application traits of remote sensing data at each scale.

C. PLB monitoring model based on machine learning and spectral indices

To detect PLB, a suite of machine learning algorithms(introduced in Section II) were employed to construct the PLB monitoring model, with a thorough performance evaluation. After normalizing the predictive indicators, the comparative results of seven machine learning models are visually presented in Fig. **9**. RF and CatBoost perform well in regression, exhibiting lower RMSE and higher R-square values. Their ability to capture complex relationships within the data suggests a complex relationship

between PLB severity and spectral features. XGBoost performs well in classification, demonstrating higher Accuracy, Precision, Recall, and F1 score. While CatBoost is perform well in regression, exhibiting lower RMSE and higher R-square values. Their ability to capture complex relationships within the data suggests a complex relationship between PLB severity and spectral features. XGBoost performs well in classification, demonstrating higher Accuracy, Precision, Recall, and F1 score. While CatBoost is comparable in these metrics, XGBoost slightly outperformed in Precision and Recall. Overall, XGBoost demonstrates superior performance on the dataset, particularly in classification, indicating its higher feasibility and practicality for satellite-scale monitoring compared to regression methods.

The XGBoost model's feature importance evaluation results show that the importance score of the DWSI2 feature is significantly higher than of other features (Fig. **10**), indicating its crucial role in predicting the target variable. Compared to previous studies, our research further emphasizes the importance of DWSI2, providing new insights for relevant work in the field. This finding enhances the understanding of machine learning methods for PLB monitoring and offers valuable information for satellite-scale monitoring. The computation of the DWSI2 index provides information about vegetation chlorophyll, moisture status, and land characteristics. Specifically, the numerator's red edge index minus the green band represents the specific reflection characteristics of the potato canopy, while the denominator involves combinations of SWIR1 and red bands. This comprehensive approach captures the reflection characteristics of both the potato canopy and land surface. DWSI2 is particularly effective in capturing features relevant to PLB monitoring, exhibiting high importance among various bands used in XGBoost machine learning modeling.

Thus, the PLB monitoring model, integrating of spectral indices and XGBoost algorithm (PLB-SI-XGBoost) was proposed for the ground-scale PLB prediction. Firstly, 596 high-quality ground data from the data source were divided into training and testing sets with a ratio of 4 to 1. To find the optimal model configuration,a grid search was conducted in the hyperparameter space. The hyperparameters such as learning rate, number of trees, maximum depth, subsample ratio, and column sampling ratio were all considered. The optimal combination was determined with a learning rate of 0.2, 50 trees, maximum depth of 3, subsample ratio of 0.8, and a column sampling ratio of 1.0.

To evaluate the PLB-SI-XGBoost model's generalization ability, the model was then applied to the testing set and the RMSE and five-fold cross-validated R-square value were calculated. The five-fold cross-validation results (Table **IV**) show excellent performance, with an RMSE of approximately 12.09 and an R-square of 0.98 on the training set. On the validation set, an MSE of 184.18, an R^2 of 0.88, and an RMSE of approximately 13.50 were observed. Overall, the proposed model performed well on the training set and exhibited relatively good performance on the validation set, demonstrating strong prediction performance and generalization ability for PLB.

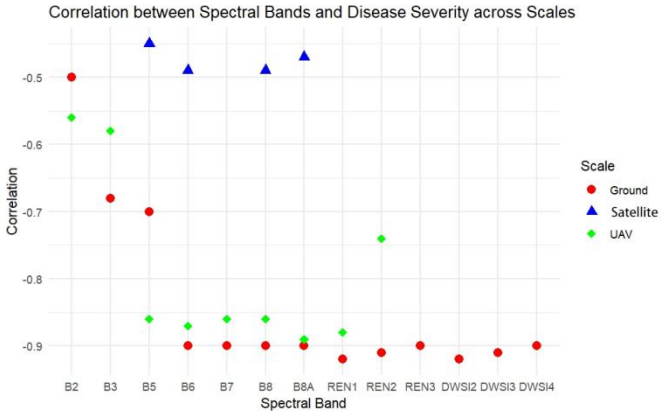

Fig. 8. Differential performance of the correlation between spectral data and PLB severity at different scales (ground, UAV, satellite) with a significance level of 0.001.

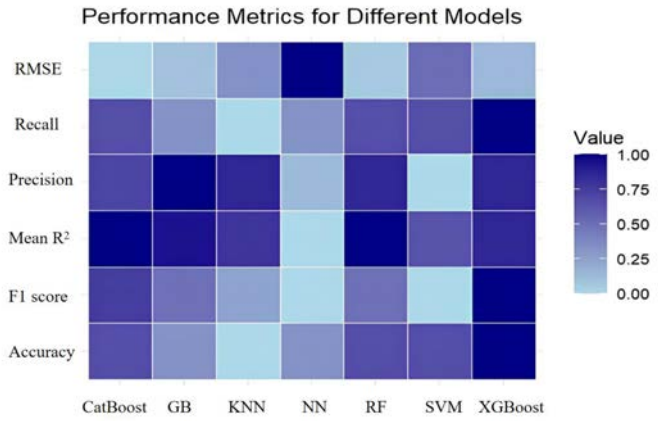

Fig. 9. Comparative analysis of seven models integrating spectral indices and machine learning algorithms

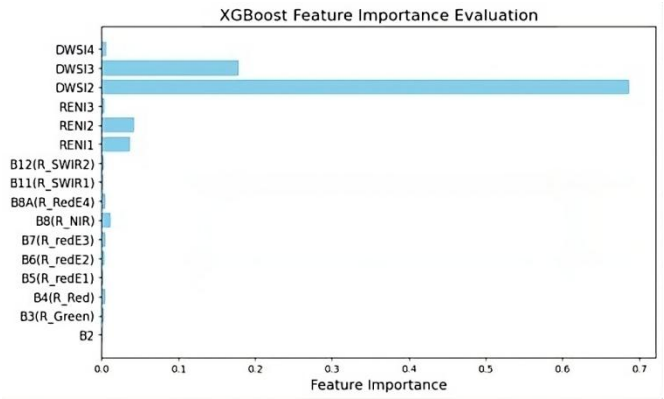

Fig. 10. Feature importance of the PLB-SI-XGBoost model based on the ground obersvation.

TABLE Ⅳ

THE DIFFERENT PERFORMANCES OF THE MODEL BASED ON

GROUND-SCALE TRAINING SET AND THE VALIDATION SET

	Training set	Validation set
(RMSE)	12.09	13.50
(R^2)	0.98	0.88

To further validate the effectiveness of the model, the relationship between the PLB-SI-XGBoost model predictions and the actual observations is shown in **Fig. 11**. Most of the scatter is distributed around the diagonal line, indicating that the model effectively captures overall trends and changes in the data and accurately predicts the target variable in most cases. However, some discrete points were also observed, which could be outliers or instances of poor model performance. Overall, the comparison chart between prediction and reality reflects the model's performance, providing an important clue for evaluating the accuracy and reliability of the model. This indicates a generally favorable modeling effect.

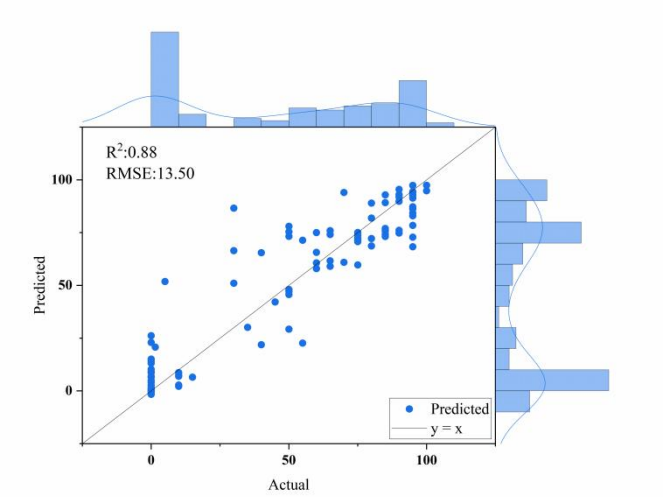

Fig. 11. Comparison of the actual value with the prediction by the PLB-SI-XGBoost model trained at the ground-scale.

D. Verification of the model at the UAV and satellite scale

The PLB-SI-XGBoost model developed at ground scale, was then validated at the UAV and satellite scale, respectively.

1). *UAV-scale verification*

The validation results show an R-square of up to 0.74, and an RMSE of 18.27. The model performs well in UAV-scale regression and demonstrates robust generalization ability.

The predicted values and the corresponding actual observed values for each sample are shown in Fig. **12**. Most of the scatter points are distributed around the diagonal, indicating that the model's predictions are in good agreement with reality and accurately predict the target variable in most cases. However, some discrete points, especially those with low disease levels, were observed. These discrete values could be outliers or samples where the model underperforms at low PLB levels.

2). Satellite-scale verification

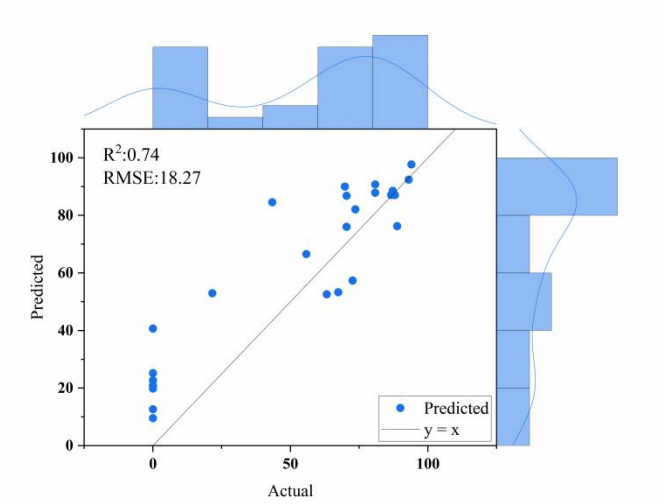

Fig. 12. Comparison of the actual value and the prediction by the PLB-SI-XGBoost model trained at the UAV scale.

The accuracy of the PLB-SI-XGBoost model trained at ground scale was verified using Sentinel-2 data and field observation data in different regions. As shown in Fig. **13,** the 70% accuracy prediction for PLB indicates a good overall classification performance. The model demonstrated a precision of 65%, meaning that 65% of the samples predicted as infected were indeed infected, indicating a low misjudgment rate. Additionally, the model showed a recall rate of 70%, effectively capturing real infection samples and reducing the possibility of missed diagnoses, which is beneficial for disease control. Considering both accuracy and recall, the F1 score reaches 66%, highlighting the comprehensive performance evaluation of the model and providing useful guidance for balancing the accuracy and comprehensiveness of the predictions.

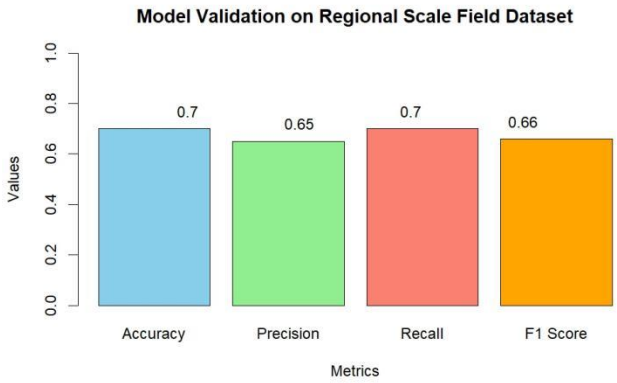

Fig. 13. The validation results of the PLB-SI-XGBoost model at the satellite scale.

The confusion matrix (Fig. **14**) shows that 116 samples in the first category (disease severity 0-25) were accurately classified, 1 sample was incorrectly classified as the second category, and 9 were misclassified as the third category. For the second category (disease severity 25-50), only 1 out of 20

samples were correctly classified, 1sample was misclassified as the first category, and 2 were misclassified as the third category. For the third category (disease severity 50-100), 23 out of 51 samples were accurately classified, 4 were misclassified as the first category, and 24 were misclassified as the second category. In general, the model demonstrates a good classification performance for samples with a disease degree of 0-25, and there is a certain degree of misclassification for samples with severity of 25-50 and 50-100. The results indicate that PLB can be better detected at an early stage when the disease severity is low, which can support intelligent and efficient decision-making in agricultural production , thereby reducing losses and costs.

In addition,the spatial distribution of errors in the PLB-SI-XGBoost model is visualized (Fig. **15**). Overall, the model performs well in predicting the severity of PLB, facilitating early-stage PLB monitoring, and providing decision support to minimize further delays.

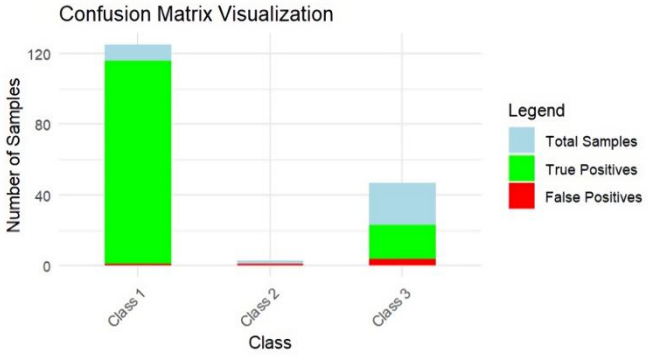

Fig. 14. Confusion matrix results of the PLB-SI-XGBoost model for the severity classification of PLB in study area. (Class 1:0-25; Class 2:25-50; Class 3:50-100).

IV. Discussion

A. Validity and Universality Across Scales

The scale problem is the core problem of remote sensing [42, 43] , and the scale effect is especially obvious in the classification accuracy of remote sensing images [44, 45]. Studies have shown that increasing the spatial resolution of an image can reduce the number of mixed pixels and thus improve the classification accuracy [46, 47]. However, as the spatial resolution is further increased, the spectral variability within the same category increases, which in turn may lead to a reduction in classification accuracy [48]. This suggests that the choice of scale is critical to the accuracy of remotely sensed data, which raises concerns about the scalability of ground-scale models. In this study, the proposed model was validated at multiple scales, including ground, UAV, and satellite. Ground (0.2m ×0.2m) and UAV(1m×1m) data can provide detailed information, more effectively capturing micro-scale spectral variations associated with disease severity compared to satellite data (10m×10m). Our results indicate that the validation accuracy of proposed model is highest at the ground scale (0.88), followed by the UAV scale (0.74), and the lowest at the satellite scale (0.70). This discrepancy may be mainly due to spatial resolution and scale effects, which are consistent with the findings of Song et al [49]. In addition, atmospheric conditions and other environmental factors may affect the spectral features captured by the sensors. Satellite data may be more susceptible to atmospheric interference, which may affect the accuracy of the models. The timing of data collection relative to disease progression and environmental conditions may affect model performance. UAV and satellite data may be acquired at different times, resulting in differences in disease spectral expression. The study aims to extend PLB monitoring model built at ground scale to the satellite scale, focusing on universal systemic rules and optimal scale identification. Ground scale can offer high accuracy, UAV enable quantitative disease assessment, while satellites, despite limited classification capabilities, can identify PLB in early stages over large areas quickly and cost-effectively. Furthermore, the study posits that while remote sensing data exhibits a general pattern and broad applicability, it is crucial to account for scale effects and other influential factors when interpreting data at different scales.

B. Model Generalization for large area

Validation at UAV and satellite scales demonstrate the model's robustness and generalizability. The model's success in UAV regression and 70% disease detection accuracy on satellite-scale Sentinel-2 data suggest its potential for broader applications. Comprehensive generalization validation across diverse seasons, climates, and soil conditions is essential to assess model performance and enhance applicability. Future research could explore deep learning algorithms for improved handling of satellite-scale data and complex relationships.

C. Superiority and Limitations of Machine Learning Algorithms

This study highlights the superior performance of the XGBoost model in PLB monitoring, as evidenced by high R-square values and low RMSE in training and validation sets. As a gradient boosting variant, XGBoost excels at capturing multivariable relationships, potentially offering better insights into spectral reflectance differences. However, the "black-box" nature of machine learning algorithms [50] may limit interpretability, posing challenges in explaining sensitive band discrepancies and evaluating feature importance, such as DWSI2.

D. Constraints Due to Data Limitations

The proposed model, which focuses on specific regions and growth stages, faces challenges in obtaining high-quality, satellite-corresponding ground observation data across multiple time frames. Similarly, the limited number of authentic samples within the UAV dataset presents difficulties in rigorously validating the model's efficacy. Expanding study areas and covering more growth stages could improve model generalization. The spatial resolution of satellite data can limit the effectiveness of disease surveillance.

E. Disease Severity Classification and Future Directions

The refinement of disease severity classification can offer more precise agricultural recommendations. A detailed classification system helps in accurately understand disease conditions and carry out appropriate management. The extensive use of Sentinel-2 and other high remote sensing data necessitates further model or algorithm optimization. Specifically, we can try to improve the resolution and frequency of satellite data, integrate multisource remote sensing and environmental data, explore radar data for enhancing accuracy and practicality of monitoring. Ensuring the robustness of the model in different climates and geographical locations is also a key direction for future work.

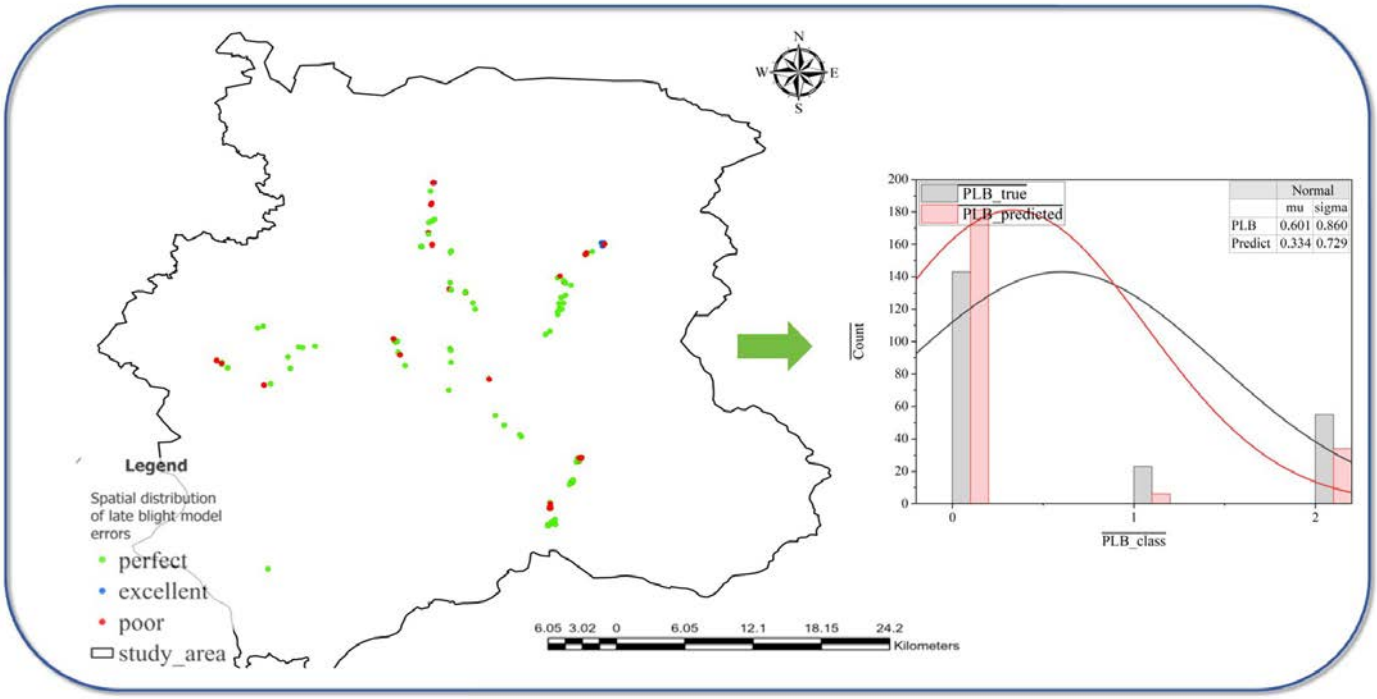

Fig. 15. Spatial distribution of the error of the PLB-SI-XGBoost model on August 12, 2021. The error is calculated as the absolute difference between the predicted value and the field data: green represents perfect model performance, blue represents excellent performance, and red represents poor performance.

V. Conclusion

By integrating technological solutions, this study fills the gap in satellite-scale PLB monitoring, enhancing the agricultural decision-making process. The multi-scale data analysis underscores the effectiveness of machine learning algorithms and remote sensing technologies in detecting PLB over large areas. This research employs a synergistic approach, combining ground experiments, UAV spectral data, and satellite imagery, to overcome the limitations inherent in traditional monitoring methods.

This study is the first to emphasize the consistency in spectral reflectance trends across ground, UAV, and satellite scales. These trends include specific band valleys and peaks, and the overall shape of the spectral reflectance curves. The red edge and near-infrared bands exhibit universal sensitivity to PLB detection across scales, highlighting the importance of these bands in spectral analysis. As disease severity increases, there is a general decrease in reflectance for specific bands (B6, B7, B8, B8A), with varying degrees of reduction corresponding to different levels of disease severity.

The study also explores scale-dependent spectral variations, revealing that as PLB severity increases, the spectral values at the ground scale, especially in bands B6, B7, B8, and B8A, exhibit more pronounced changes compared to those observed at UAV and satellite scales. UAV-derived spectral curves show a narrower bandwidth and some gaps, possibly due to limitations in the spatial resolution and data capture continuity of UAV sensors. Compared to satellite systems, the spectral values at ground and UAV scales are similar, while the satellite scale shows wider upper and lower limits. Generally, it notes that scale effects may influence the generalizability of predictive models. While the ground scale provides the highest accuracy, UAV and satellite scales are equally effective for disease monitoring, offering a robust framework for multi-scale disease detection.

Furthermore, based on the developed Red Edge Index and Disease Stress Index with a suite of machine learning algorithms, a PLB-SI-XGBoost model was proposed. Notably, the proposed model demonstrated the highest average evaluation score of 0.88 and the lowest RMSE of 13.50 during ground scale validation, outperforming other algorithms. At the UAV scale, the proposed model achieved a robust R-squared value of 0.74 and an RMSE of 18.27.

Moreover, the application of Sentinel-2 data for disease detection at satellite scale yielded an accuracy of 70% in the model. Overall, the PLB-SI-XGBoost model demonstrated its exceptional generalization capabilities.

The research indicates that although monitoring patterns demonstrate a degree of universality and systematicity across scales, the strength of correlation may weaken as the scale expands. Satellite remote sensing emerges as a promising method for large scale monitoring, laying a solid foundation for the integration of machine learning with remote sensing techniques. Future studies should focus on refining model algorithms and enhancing the resolution and frequency of satellite data to improve the precision and applicability of PLB monitoring. In conclusion, this study pioneers new avenues for disease monitoring in satellite-scale agricultural production, paving the way for enhanced agricultural efficiency, minimized resource wastage, and the advancement towards Agriculture 4.0.

REFERENCES

[1] B. Liu et al., "Promoting potato as staple food can reduce the carbon–land–water impacts of crops in China," Nature Food, vol. 2, no. 8, pp. 570-577, 2021/08/01 2021, doi: 10.1038/s43016-021-00337-2.

[2] C. Gao et al., "Pathogen manipulation of chloroplast function triggers a light-dependent immune recognition," Proceedings of the National Academy of Sciences, vol. 117, no. 17, p. 202002759, 2020.

[3] F. C. Bawden, "Infra-Red Photography and Plant Virus Diseases," Nature, vol. 132, no. 3326, pp. 168-168, 1933/07/01 1933, doi: 10.1038/132168a0.

[4] D. Moshou et al., "Plant disease detection based on data fusion of hyper-spectral and multi-spectral fluorescence imaging using Kohonen maps," Real-Time Imaging, vol. 11, no. 2, pp. 75-83, 2005.

[5] E. C. Davis, "A review of advanced techniques for detecting plant diseases," Computers and Electronics in Agriculture, 2010.

[6] A. Dutta et al., "Early detection of wilt in Cajanus cajan using satellite hyperspectral images: Development and validation of disease-specific spectral index with integrated methodology," Computers and Electronics in Agriculture, vol. 219, p. 108784, 2024/04/01/ 2024, doi: https://doi.org/10.1016/j.compag.2024.108784.

[7] L. Tian et al., "A disease-specific spectral index tracks Magnaporthe oryzae infection in paddy rice from ground to space," Remote Sensing of Environment, vol. 285, p. 113384, 2023/02/01/ 2023, doi: https://doi.org/10.1016/j.rse.2022.113384.

[8] L. Wan, H. Li, C. Li, A. Wang, Y. Yang, and P. Wang, "Hyperspectral Sensing of Plant Diseases: Principle and Methods," Agronomy, vol. 12, no. 6, p. 1451, 2022. [Online]. Available: https://www.mdpi.com/2073-4395/12/6/1451.

[9] J. Rodríguez, I. Lizarazo, F. Prieto, and V. Angulo-Morales, "Assessment of potato late blight from UAV-based multispectral imagery," Computers and Electronics in Agriculture, vol. 184, p. 106061, 2021/05/01/ 2021, doi: https://doi.org/10.1016/j.compag.2021.106061.

[10] J. Zhang et al., "Monitoring plant diseases and pests through remote sensing technology: A review," Computers and Electronics in Agriculture, vol. 165, p. 104943, 2019/10/01/ 2019, doi: https://doi.org/10.1016/j.compag.2019.104943.

[11] L. Liu et al., "A Disease Index for Efficiently Detecting Wheat Fusarium Head Blight Using Sentinel-2 Multispectral Imagery," IEEE Access, vol. 8, pp. 52181-52191, 2020.

[12] X. Jing, Q. Zou, J. Yan, Y. Dong, and B. Li, "Remote Sensing Monitoring of Winter Wheat Stripe Rust Based on mRMR-XGBoost Algorithm," Remote Sensing, vol. 14, no. 3, p. 756, 2022. [Online]. Available: https://www.mdpi.com/2072-4292/14/3/756.

[13] M. H. D. Franceschini, H. Bartholomeus, D. F. Van Apeldoorn, J. Suomalainen, and L. Kooistra, "Feasibility of Unmanned Aerial Vehicle Optical Imagery for Early Detection and Severity Assessment of Late Blight in Potato," Remote Sensing, vol. 11, no. 3, 2019.

[14] M. Zhang, Z. Qin, X. Liu, and S. L. Ustin, "Detection of stress in tomatoes induced by late blight disease in California, USA, using hyperspectral remote sensing," International Journal of Applied Earth Observations & Geoinformation, vol. 4, no. 4, pp. 295-310, 2003.

[15] D. Bienkowski, Matt J.Lees, Alison K.Gallagher, ChristopherNeilson, Roy, "Detection and differentiation between potato (Solanum tuberosum) diseases using calibration models trained with non-imaging spectrometry data," Computers and Electronics in Agriculture, vol. 167, 2019.

[16] S. Appeltans, J. G. Pieters, and A. M. Mouazen, "Potential of laboratory hyperspectral data for in-field detection of Phytophthora infestans on potato," PRECISION AGRICULTURE, vol. 23, no. 3, pp. 876-893, JUN 2022, doi: 10.1007/s11119-021-09865-0.

[17] J. Kool, T. H. Been, and A. Evenhuis, "Detection of Latent Potato Late Blight by Hyperspectral Imaging," 2021 11th Workshop on Hyperspectral Imaging and Signal Processing: Evolution in Remote Sensing (WHISPERS), pp. 1-5, 2021.

[18] C. I. Fernandez, B. Leblon, A. Haddadi, J. F. Wang, and K. Wang, "Potato Late Blight Detection at the Leaf and Canopy Level Using Hyperspectral Data," CANADIAN JOURNAL OF REMOTE SENSING, vol. 46, no. 4, pp. 390-413, JUL 3 2020, doi: 10.1080/07038992.2020.1769471.

[19] C. Roy et al., "Microbiome and ecology of a hot spring-microbialite system on the Trans-Himalayan Plateau," Scientific Reports, vol. 10, no. 1, Apr 2020, Art no. 5917, doi: 10.1038/s41598-020-62797-z.

[20] Y. Shi, L. Han, A. Kleerekoper, S. Chang, and T. Hu, "Novel CropdocNet Model for Automated Potato Late Blight Disease Detection from Unmanned Aerial Vehicle-Based Hyperspectral Imagery," Remote Sensing, vol. 14, no. 2, doi: 10.3390/rs14020396.

[21] L. Yuan, J. Zhang, Y. Shi, C. Nie, L. Wei, and J. Wang, "Damage Mapping of Powdery Mildew in Winter Wheat with High-Resolution Satellite Image," Remote. Sens., vol. 6, pp. 3611-3623, 2014.

[22] Z. Qiong, H. Wenjiang, C. Ximin, S. Yue, and L. Linyi, "New Spectral Index for Detecting Wheat Yellow Rust Using Sentinel-2 Multispectral Imagery," Sensors, vol. 18, no. 3, p. 868, 2018.

[23] J. Duarte-Carvajalino, D. Alzate, A. Ramirez, J. Santa-Sepulveda, A. Fajardo-Rojas, and M. Soto-Suárez, "Evaluating Late Blight Severity in Potato Crops Using Unmanned Aerial Vehicles and Machine Learning Algorithms," Remote Sensing, vol. 10, no. 10, pp. 1513-, 2018.

[24] H. Sun et al., "Potato late blight severity monitoring based on the relief-mRmR algorithm with dual-drone cooperation," Computers and Electronics in Agriculture, vol. 215, p. 108438, 2023/12/01/ 2023, doi: https://doi.org/10.1016/j.compag.2023.108438.

[25] I. Iglesias, O. Escuredo, C. Seijo, and J. Méndez, "Phytophthora infestans Prediction for a Potato Crop," American Journal of Potato Research, vol. 87, no. 1, pp. 32-40, 2010/02/01 2010, doi: 10.1007/s12230-009-9114-y.

[26] R. Sugiura et al., "Field phenotyping system for the assessment of potato late blight resistance using RGB imagery from an unmanned aerial vehicle," Biosystems Engineering, vol. 148, pp. 1-10, 2016.

[27] N. Gorelick, M. Hancher, M. Dixon, S. Ilyushchenko, D. Thau, and R. Moore, "Google Earth Engine: Planetary-scale geospatial analysis for everyone," Remote Sensing of Environment, vol. 202, pp. 18-27, 2017/12/01/ 2017, doi: https://doi.org/10.1016/j.rse.2017.06.031.

[28] D. Bienkowski, M. J. Aitkenhead, A. K. Lees, C. Gallagher, and R. Neilson, "Detection and differentiation between potato (Solanum tuberosum) diseases using calibration models trained with non-imaging spectrometry data," Computers and Electronics in Agriculture, vol. 167, p. 105056, 2019/12/01/ 2019, doi: https://doi.org/10.1016/j.compag.2019.105056.

[29] S. S. Ray, N. Jain, R. K. Arora, S. Chavan, and S. Panigrahy, "Utility of Hyperspectral Data for Potato Late Blight Disease Detection," Journal of the Indian Society of Remote Sensing, vol. 39, no. 2, pp. 161-169, 2011.

[30] I. Filella and J. Penuelas, "The red edge position and shape as indicators of plant chlorophyll content, biomass and hydric status," International Journal of Remote Sensing, vol. 15, no. 7, pp. 1459-1470, 1994/05/10 1994, doi: 10.1080/01431169408954177.

[31] T. Zheng et al., "Estimation of Chlorophyll Content in Potato Leaves Based on Spectral Red Edge Position," IFAC-PapersOnLine, vol. 51, no. 17, pp. 602-606, 2018/01/01/ 2018, doi: https://doi.org/10.1016/j.ifacol.2018.08.131.

[32] L. S. Galvão, A. R. Formaggio, and D. A. Tisot, "Discrimination of sugarcane varieties in Southeastern Brazil with EO-1 Hyperion data," Remote Sensing of Environment, vol. 94, pp. 523-534, 2005.
[33] L. Breiman, "Random Forests," Machine Learning, vol. 45, no. 1, pp. 5-32, 2001/10/01 2001, doi: 10.1023/A:1010933404324.
[34] R. Lawrence, A. Bunn, S. Powell, and M. Zambon, "Classification of remotely sensed imagery using stochastic gradient boosting as a refinement of classification tree analysis," Remote Sensing of Environment, vol. 90, no. 3, pp. 331-336, 2004/04/15/ 2004, doi: https://doi.org/10.1016/j.rse.2004.01.007.
[35] Y.-H. Lee, C.-P. Wei, T.-H. Cheng, and C.-T. Yang, "Nearest-neighbor-based approach to time-series classification," Decision Support Systems, vol. 53, no. 1, pp. 207-217, 2012/04/01/ 2012, doi: https://doi.org/10.1016/j.dss.2011.12.014.
[36] K. M. He, X. Y. Zhang, S. Q. Ren, J. Sun, and Ieee, "Deep Residual Learning for Image Recognition," presented at the 2016 IEEE CONFERENCE ON COMPUTER VISION AND PATTERN RECOGNITION (CVPR), 2016.
[37] V. N. Vapnik, "The Nature of Statistical Learning Theory," Springer, 1995.
[38] T. Chen and C. Guestrin, "XGBoost: A Scalable Tree Boosting System," Proceedings of the 22nd ACM SIGKDD International Conference on Knowledge Discovery and Data Mining, 2016.
[39] L. Prokhorenkova, G. Gusev, A. Vorobev, A. V. Dorogush, and A. Gulin, "CatBoost: unbiased boosting with categorical features," 2017.
[40] E. van den Heuvel and Z. Zhan, "Myths About Linear and Monotonic Associations: Pearson ' s r, Spearman ' s ρ , and Kendall ' s τ ," The American Statistician, vol. 76, no. 1, pp. 44-52, 2022/01/02 2022, doi: 10.1080/00031305.2021.2004922.
[41] S. Raschka, "Model Evaluation, Model Selection, and Algorithm Selection in Machine Learning," 2018.
[42] H. Wu and Z.-L. Li, "Scale Issues in Remote Sensing: A Review on Analysis, Processing and Modeling," Sensors, vol. 9, no. 3, pp. 1768-1793, 2009. [Online]. Available: https://www.mdpi.com/1424-8220/9/3/1768.
[43] L. I. Xiaowen and W. Yiting, "Prospects on future developments of quantitative remote sensing," Acta Geographica Sinica, vol. 68, no. 9, pp. 1163-1169, 2013.
[44] K. Xu, Q. Tian, Y. Yang, J. Yue, and S. Tang, "How up-scaling of remote-sensing images affects land-cover classification by comparison with multiscale satellite images," International Journal of Remote Sensing, vol. 40, no. 7, pp. 2784-2810, 2019/04/03 2019, doi: 10.1080/01431161.2018.1533656.
[45] R. Li, X. Gao, F. Shi, and H. Zhang, "Scale Effect of Land Cover Classification from Multi-Resolution Satellite Remote Sensing Data," Sensors, vol. 23, no. 13, p. 6136, 2023. [Online]. Available: https://www.mdpi.com/1424-8220/23/13/6136.
[46] J. Chen et al., "The Effects of Spatial Resolution and Resampling on the Classification Accuracy of Wetland Vegetation Species and Ground Objects: A Study Based on High Spatial Resolution UAV Images," Drones, vol. 7, no. 1, p. 61, 2023. [Online]. Available: https://www.mdpi.com/2504-446X/7/1/61.
[47] F. Waldner, G. Duveiller, and P. Defourny, "Local adjustments of image spatial resolution to optimize large-area mapping in the era of big data," International Journal of Applied Earth Observation and Geoinformation, vol. 73, pp. 374-385, 2018/12/01/ 2018, doi: https://doi.org/10.1016/j.jag.2018.07.009.
[48] L. Wang, C. Shi, C. Diao, W. Ji, and D. Yin, "A survey of methods incorporating spatial information in image classification and spectral unmixing," International Journal of Remote Sensing, vol. 37, no. 16, pp. 3870-3910, 2016/08/17 2016, doi: 10.1080/01431161.2016.1204032.
[49] G. Song et al., "Scale matters: Spatial resolution impacts tropical leaf phenology characterized by multi-source satellite remote sensing with an ecological-constrained deep learning model," Remote Sensing of Environment, vol. 304, p. 114027, 2024/04/01/ 2024, doi: https://doi.org/10.1016/j.rse.2024.114027.
[50] M. T. Ribeiro, S. Singh, and C. Guestrin, ""Why Should I Trust You?": Explaining the Predictions of Any Classifier," presented at the Proceedings of the 22nd ACM SIGKDD International Conference on Knowledge Discovery and Data Mining, San Francisco, California, USA, 2016. [Online]. Available: https://doi.org/10.1145/2939672.2939778.

Sheng Chang received the Ph.D. degree in remote sensing of resources and environment from the Central South University and Chinese Academy of Sciences, in 2018. He joined the Aerospace Information Research Institute, Chinese Academy of Sciences, Beijing, China, in 2009.

He has published more than 40 papers, gained 10 invention patents and 7 software copyrights as well as published 11 monographs as the main author. His research interests include surface parameters inversion at multi-scale, agricultural and water resource remote sensing, as well as in the monitoring and prediction of agricultural disasters.

Zelong Chi received his bachelor's degree in geography from Taiyuan Normal University in 2023. He is currently pursuing the M.S. degree in ecology at Tibet University and is a visiting student at the State Key Laboratory of Remote Sensing Science, Chinese Academy of Sciences.

His research interests include quantitative remote sensing in agriculture and remote sensing monitoring of potatoes.

Hong Chen received the Ph.D. degree from the Institute of Geographic Sciences and Natural Resources Research, Chinese Academy of Sciences, Beijing, China, in 2018.

She is currently an senior Engineer with China Aero Geophysical Survey and Remote Sensing Center for Nature Resources. Her research interest mainly focuses on the scaling of remotely sensed products and surface parameters inversion.

Tongle Hu received the Ph.D. degree in phytopathology from Hebei Agricultural University, Baoding, Hebei, China, in 2006.

He is currently a Professor with the College of Plant Protection, Hebei Agricultural University. His research interests include research and application of plant disease monitoring by remote sensing, and epidemiology and forecasting.

Caixia Gao received the Ph.D. degree in cartography and geography information system from the University of Chinese Academy of Sciences, Beijing, China, in 2012.

She is currently a Professor with the Aerospace Information Research Institute,

Chinese Academy of Sciences. Her research interests include in-orbit calibration and validation of optical sensors, and the retrieval of surface temperature and emissivity.

Jihua Meng, born in 1977, received his M.S. degree in remote sensing application in mineral exploration from Xinjiang University in 2003 and Ph.D. degree in Cartography and GIS in 2006 from Institute of Remote Sensing and Digital Earth in 2006.

He is currently a professor at the Aerospace Information Research Institute, Chinese Academy of Sciences. He is the author of more than 130 papers. His current research interests is remote sensing application in agriculture.

Liangxiu Han received the Ph.D. degree in computer science from Fudan University, Shanghai, China, in 2002.

She is currently a Professor of computer science with the Department of Computing and Mathematics, Manchester Metropolitan University, Manchester, U.K. Her research areas mainly lie in the development of novel big data analytics and development of novel intelligent architectures that facilitates big data analytics as well as applications in different domains.